LA-UR-15-22257
Approved for public release; distribution is unlimited.

Title: Influence of sweeping detonation-wave loading on damage evolution during spallation loading of tantalum in both a planar and curved geometry

Author(s): Gray, George Thompson III
Hull, Lawrence Mark
Livescu, Veronica
Faulkner, James
Briggs, Matthew E.
Meyer, Ross Keith
Andrews, Heather Lynn
Hare, Steven John
Jakulewicz, Micah Shawn
Shinas, Michael A.

Intended for: Report

Issued: 2015-03-30

LA-UR-15-

Influence of sweeping detonation-wave loading on damage evolution during spallation loading of tantalum in both a planar and curved geometry

Campaign 2 – L2 Milestone # 5107

Milestone Objective: Provide an assessment of material damage in Tantalum due to a sweeping detonation wave for both planar and curved geometries

Milestone Deliverable: Execute HE driven experiments using PDV and shock recovery. Conduct metallurgical analysis. Material to start with is Ta. Submit data and report to ASC.

Abstract. Widespread research over the past five decades has provided a wealth of experimental data and insight concerning the shock hardening, damage evolution, and the spallation response of materials subjected to square-topped shock-wave loading profiles. However, fewer quantitative studies have been conducted on the effect of direct, in-contact, high explosive (HE)-driven Taylor wave (unsupported shocks) loading on the shock hardening, damage evolution, or spallation response of materials. Systematic studies quantifying the effect of sweeping-detonation wave loading are yet sparser. In this study, the damage evolution and spallation response of Ta is shown to be critically dependent on the peak shock stress, the geometry of the sample (flat or curved plate geometry), and the shock obliquity during sweeping-detonation-wave shock loading. Sweeping-wave loading in the flat-plate geometry is observed to: a) yield a lower spall strength than previously documented for 1-D supported-shock-wave loading, b) exhibit increased shock hardening as a function of increasing obliquity, and c) lead to an increased incidence of deformation twin formation with increasing shock obliquity. Sweeping-wave loading of a 10 cm radius curved Ta plate is observed to: a) lead to an increase in the shear stress as a function of increasing obliquity, b) display a more developed level of damage evolution, extensive voids and coalescence, and lower spall strength with obliquity in the curved plate than seen in the flat-plate sweeping-detonation wave loading for an equivalent HE loading, and c) no increased propensity for deformation twin formation with increasing obliquity as seen in the flat-plate geometry. The overall observations comparing and contrasting the flat versus curved sweeping-wave spall experiments with 1D loaded spallation behavior suggests a coupled influence of obliquity and geometry on dynamic shock-induced damage evolution and spall strength. Coupled experimental and modeling research to quantify the combined effects of sweeping-wave loading with increasingly complex sample geometries on the shockwave response of materials is clearly crucial to providing the basis for developing and thereafter validation of predictive modeling capability.

Influence of sweeping detonation-wave loading on damage evolution during spallation loading of tantalum in both a planar and curved geometry

G.T. Gray III, L.M. Hull, V. Livescu, J.R. Faulkner, M.E. Briggs, R.K. Meyer
H. Andrews, S. Hare, M. Jakulewicz, M. Shinas

Los Alamos National Laboratory, Los Alamos, New Mexico, 87544, USA

1 Introduction

Over the past five decades numerous studies have provided a wealth of experimental data and insight concerning shock hardening and the spallation response of materials subjected to square-topped shock-wave loading profiles[1 , 2 , 3]. Fewer researchers have quantified the effect of direct, in-contact, high explosive (HE)-driven Taylor wave (or triangular-wave) loading on the shock hardening, damage evolution, or spallation response of materials[4, 5]. Direct in-contact high-explosive loading induces an impulse dubbed a "Taylor Wave". Direct explosive loading imparts a significantly different loading history than that achieved by a square-topped impulse in terms of both the pulse duration at a fixed peak pressure, and a different unloading strain rate from the peak Hugoniot state achieved[6]. Seminal studies by Rinehart[7], and Butcher *et al*.[6] detailed how the formation and thickness of the "scabbing under explosive loading" (*i.e*. spallation), depends directly on the shape of the stress wave imposed. Butcher *et al*.[6] demonstrated that "since spallation is studied by introducing a pulse and observing the effects of the tensile stresses within the material, knowledge of the stress history at the spall plane is necessary to the quantitative understanding of spall". Further, experiments by Butcher *et al*.[6] revealed "that the spallation stress is less for square pulses than for triangular pulses".

Later studies by Al'tshuler, Novikov, and Divnov [8] summarized direct explosively-driven spallation experiments stating that "the resistance of metal to fracture in the case of a strong blow or explosion is not a constant characteristic of its strength, but rather may vary over a wide range depending on the pressure gradient (or on strain rate) in the interacting rarefaction waves". Additional experiments by Drummond[9] and more recently Ogorodnikov *et al*.[10] has led to an increased emphasis on research in HE-driven spallation due to oblique loading via sliding detonation waves.

Recent sweeping-detonation-wave shock-loading and spallation experiments on Cu have shown that based on variations in the specifics of the shock drive (pulse shape, peak stress, shock obliquity) and sample geometry, "spall strength" in High-purity Cu varies by over a factor of two and the details of the mechanisms of the damage evolution are seen to vary[2]. Divergent direct PETN explosive loading of Ta revealed that Ta twin formation during shock loading in Ta is a strong function of shock obliquity. This is consistent with the effect of obliquity on the imposed stress tensor during shock loading that effectively varies the ratio of the spherical (hydrostatic) and deviatoric (shear) stress[3 , 11].

2 Experimental Procedure – Flat Plate and Curved Geometries

Targets for sweeping detonation-wave loading tests were prepared from commercially pure, triple electron-beam melted and annealed tantalum plate, 10.2 mm in thickness obtained from Cabot Corporation. The chemical composition (in wt%) was analyzed to be carbon 10 ppm, oxygen <50 ppm, nitrogen <10 ppm, hydrogen <5 ppm, tungsten <25 ppm, niobium <25 ppm, titanium <5 ppm, iron <5 ppm, and the balance Ta. The plate was produced from an ingot, which was forged into a billet; this was

then annealed, and subsequently cut prior to cross rolling. The plates were straight rolled in the final finishing passes. Cross rolling of the Ta plate resulted in divergence from the typical straight-rolled texture, from a partial to a nearly continuous γ fiber (<111>//*ND*) along with the virtual extinction of the partial α fiber (<110>//*RD*). The texture strength was moderate, with the <111> fiber component approximately eight times random. Acoustic properties of the tantalum were measured using 5 MHz quartz transducers with a Parametrics 500PR pulse receiver. The density (ρ_0) of the tantalum studied was measured to be 16.58±0.01 g/cc, longitudinal sound speed (c_L) 4.13±0.03 mm/μs and shear sound speed (c_S) 2.04±0.03 mm/μs. The Poisson ratio (ν) was 0.339.

The explosive assembly used to drive the sweeping wave into the tantalum samples for the flat planar plates is shown in Fig. 1. The samples were 10.2mm thick x 50.8 mm wide x 88.9 mm long. Equal thickness rails made of tantalum that are 25.4mm in width by 10.2mm in thickness surrounded the sample to provide relief from the transverse and end (longitudinal) rarefactions along the edges that tend to cause the edges to lag.

The explosive drive was provided by Detasheet initiated with a line wave generator. The line wave generator is made by extruding XTX explosive into tracks that form equal lateral triangles. The line wave generators have a small arrival time ripple on the output wave that corresponds to the spacing between the tracks, and the average output simultaneity is ±10 ns. Three explosive loading configurations were used to approach conditions of incipient spall. All of the experiments used 8 mm of Detasheet explosive, with varying amounts of polyurethane foam between the explosive and the tantalum. The plate thickness and the lateral dimensions of the flat-plate assemblies were not varied. In the first configuration an 8 mm thick piece of Detasheet was separated from the tantalum by a 6.35mm layer of 0.04 g/cc polyurethane foam. The second configuration used 8 mm of Detasheet that was separated from the tantalum by a 3.175mm layer of 0.25 g/cc polyurethane foam. In the third shot, the 8mm of Detasheet was placed in direct contact with the tantalum assembly. The purpose of the foam is to allow the explosive products to expand before interacting with the sample, thereby producing a reduced amplitude oblique shock in the sample.

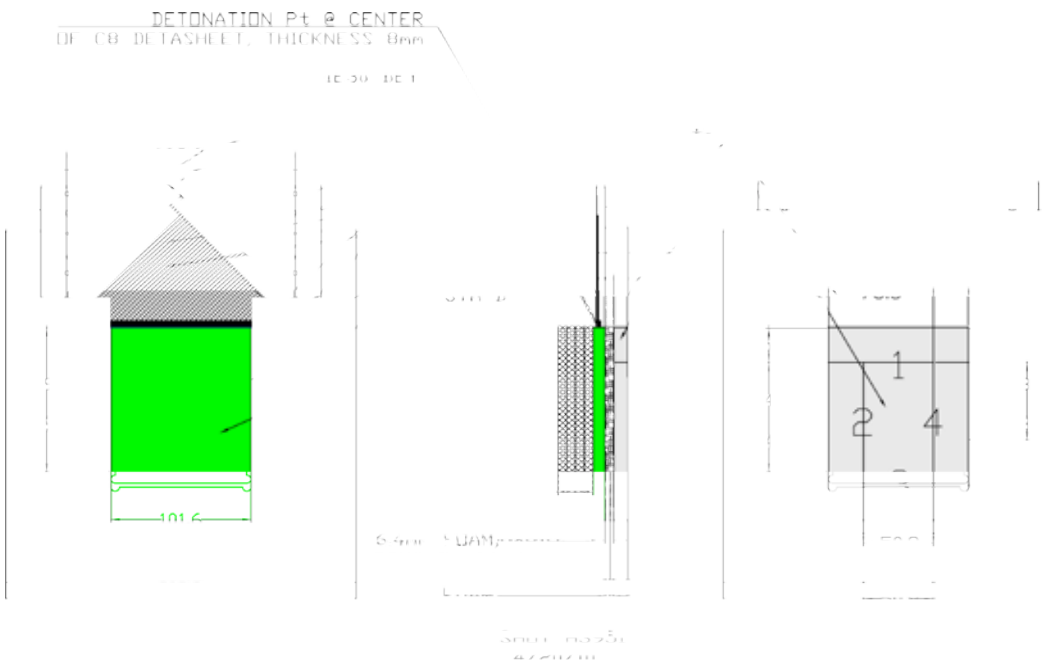

Figure 1. Three schematic views of sweeping detonation-wave shot set-up.

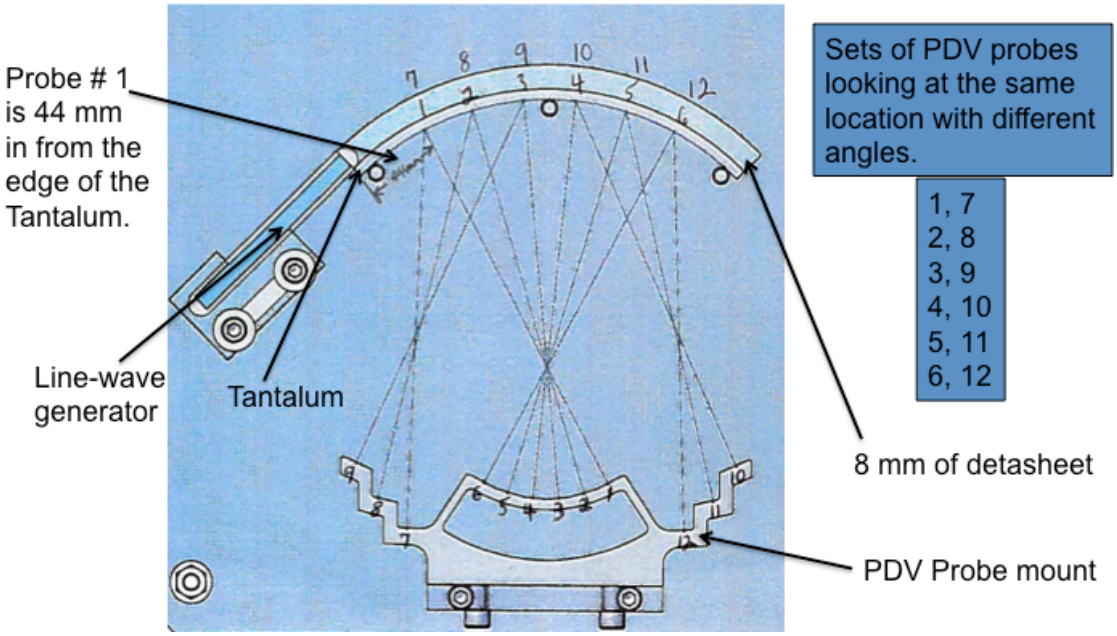

Figure 2. PDV shot configuration of 10cm radius curved Ta sweeping detonation-wave assembly.

Figure 3. 10cm radius curved Ta sweeping detonation-wave assembly set-up.

The primary diagnostics for both the flat-plate and curved-plate geometry spall experiments was sample recovery with post-mortem metallurgical analysis and Photon Doppler Velocimetry (PDV). The PDV was used to capture the velocity history of the sample at four points in an approximately square array on the flat Ta sample. The probes have a 100mm working distance and each probe interrogates a spot that is about 200 μm in diameter. The array for the flat Ta plate assembly was roughly aligned so that two pairs of points are approximately parallel to the detonation direction and the two pairs straddle

the center of the sample. The probe locations were placed at 50 and 100mm from the top surface of the Ta flat plate sample. The alignment is not expected to be exact with regard to the probe's interrogation points, but adequately perpendicular to the tantalum surface to capture good return signals.

Evaluation of the effect of curvature on the damage evolution in Ta was conducted via testing of a curved sweeping-wave spallation assembly. For the 10 cm radius curved Ta configuration, an 8 mm thick piece of Detasheet was separated from the curved tantalum by a 6.35mm layer of 0.04 g/cc polyurethane foam to replicate the lowest HE shock drive condition used on the flat-plate geometry where incipient spallation damage was observed. The details of the explosive drive, specifically the line-wave generator and detonator configurations, were kept constant with that utilized for the flat-plate experiments. For the 10 cm radius curved Ta assembly, six sets of PDV locations were set to view the curved plate. At each of the six locations two probes were set to view each location, one viewing normal to the plate surface (to register the orthogonal jump off) and one angled at 45 degrees(to track the shear particle motion). Figure 2 shows the configuration of the PDV probe layout for the 10cm curved Ta plate shot set-up and Figure 3 presents a photo of the shot assembly positioned above the water tank used to decelerate the spall assembly parts.

The Ta specimens, from both the flat-plate and 10cm radius curved geometries, following sweeping-wave loading were cross-sectioned and prepared for optical metallography and electron backscatter diffraction (EBSD)[12]. Automated EBSD scans were performed with a step size of 0.15 μm in a hexagonal grid at 20 kV in an FEI XL30 FEG-SEM equipped with TSL data acquisition hardware and software. The local misorientations as a function of location surrounding areas of interest were mapped using the EBSD data.

The objective of the recovery portion of the study was to identify and characterize the micro-mechanisms of damage evolution and observe the evolution in damage evolution during spall driven by a sweeping wave; i.e., as a function of increasing shock obliquity, and specimen geometry (flat versus curved plates), and correlate the findings with the PDV data. The objective of the velocimetry was to characterize the free surface velocity wave profiles and their differences as a function of variations in explosive drive in the case of the flat plate and geometry in the comparison between a flat and curved plate driven with the identical HE loading.

3 Results and Discussion

3.1a Post-Mortem Metallurgical Analysis – Flat-Plate Geometry

The damage evolution in energetic-driven oblique shock loading of Ta was seen to vary as a function of the imposed explosive loading intensity. Figure 4 shows macroscopic optical micrographs of the three sweeping-wave loaded samples as a function of the explosive loading set-up. Optical microscopy on tantalum specimen ***I*** indicated no defined spall plane and very incipient void damage evolved in the sample. Isolated voids up to 10μm in diameter were scattered throughout the microstructure as seen in figure 5.

The majority of these voids appear to lie on or near grain boundaries. In response to the diverging detonation wave, Ta specimen ***I*** displayed a higher density of twins near the bottom surface, away from the surface adjacent to the explosive. This is where the loading obliquity was maximum. Electron Backscattered Diffraction was used to interrogate specific regions for detection of obliquity effects as a function of distance from the detonation point on Ta specimen ***I***. Optical metallography of specimen ***I*** following etching and viewed using polarized illumination also revealed extensive dislocation pits as seen in figure 6. Preferential chemical attack due to small regions of stress with a subtly different electrode potential resolves these pits[13]. The propensity of dislocation pits to lie at or near grain

boundaries is consistent with the need to plastically accommodate the compatibility stresses between polycrystals.

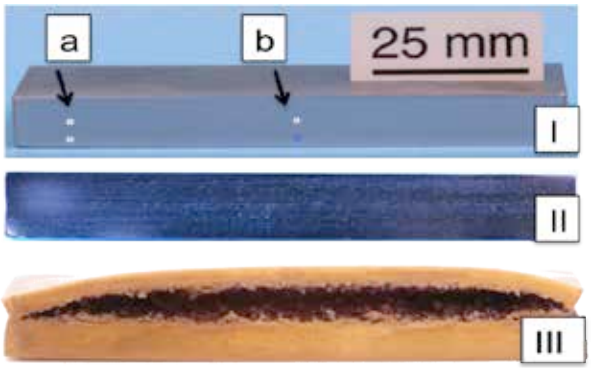

Figure 4. Macroscopic cross-sectional view of the three sweeping detonation-wave samples: I) 8mm of Detasheet with a 6.35 mm foam interlayer revealing no observable evolved damage, II) 8mm of Detasheet with 3.175mm of foam interlayer showing developing incipient spall including partial linkage and cracking between voids, and III) significant incipient spall including a single spall scab and extensive ductile tearing. The direction of the sweeping wave is from left to right in each sample.

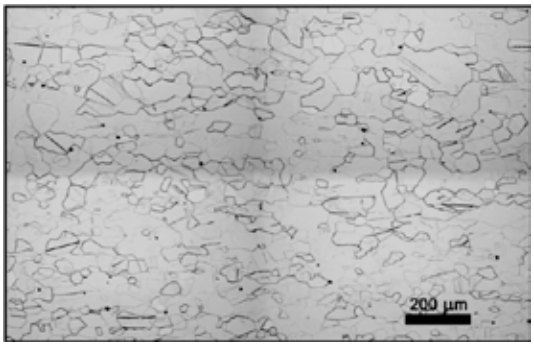

Figure 5. Isolated voids and dislocation pits in specimen ***I***.

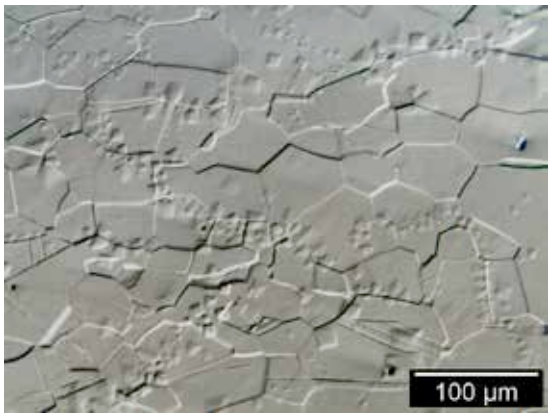

Figure 6. Optical metallography of Ta Specimen ***I*** using polarized illumination revealing dislocation etch pits preferentially located along grain boundaries.

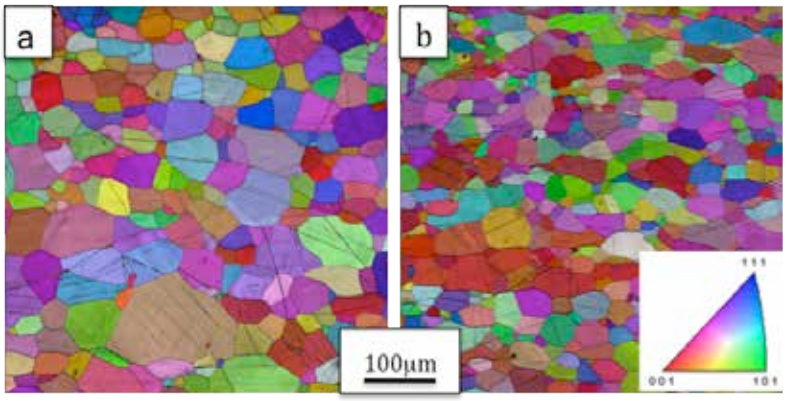

Figure 7. EBSD scans of regions 'a' and 'b' from Ta Specimen ***I*** showing minimal microstructural damage evolution due to the sweeping-wave loading with 8mm Detasheet plus 6.35mm foam.

For EBSD analysis, we selected two regions, approximately 50mm apart along the x direction. The two locations are denoted as positions 'a' and 'b' in figure 4. Two sets of scans with a step size of 0.7 microns were performed. The EBSD data indicated no microstructural differences between regions 'a' and 'b' as seen in figure 7. EBSD data analysis for specimen ***I*** also revealed essentially no microstructural disturbances around voids and minimal deformation affected material aside from the presence of twins. The usual defect indicators sought were: 1) grain orientation gradients as witnesses of anisotropic deformation, 2) enhanced localized misorientations as potential damage initiation sites, and 3) deformation twins as suggesting a change in the balance of hydrostatic and deviatoric stresses as well as potential sites for damage nucleation. However, both the crystal orientation maps and the kernel average misorientation maps were found to be similar for the two regions interrogated in specimen ***I***.

As minimal incipient spallation damage was found in specimen ***I***, the amount of the foam interlayer was reduced in the second experiment to 3.175mm while keeping the explosive thickness unchanged. Specimen ***II*** was found to exhibit a more advanced damage state and a vaguely defined spall plane as seen in figure 4. Voids were up to 200μm in diameter. While larger voids in specimen ***II*** appear round, incipient damage areas indicate that they are the result of growth and coalescence of multiple small voids. In response to the diverging detonation wave, both specimens ***I*** and ***II*** displayed a higher density of twins near the bottom edge compared to the top, and closer to the right bottom corner away from the detonation edge similar to our previous studies on Cu and Ta[2, 3]. Figure 8 shows the increased density of deformation twins formed in specimen ***II*** as a function of increased shock obliquity coincidently while the peak 'pressure' or hydrostatic component of the experiment is falling with increasing shock obliquity[11].

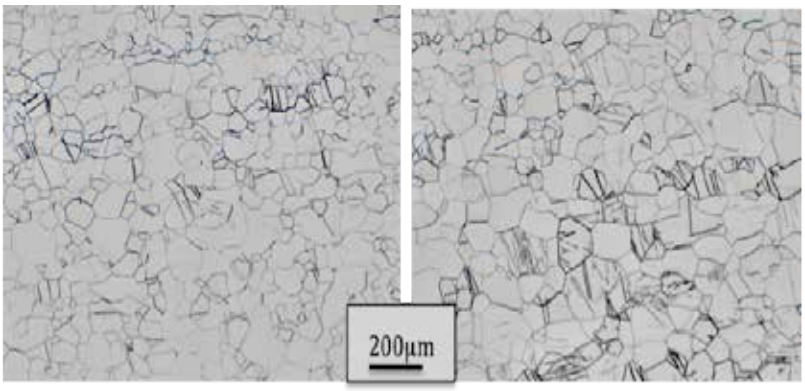

Fig. 6. Increasing propensity of deformation twin formation in Ta specimen ***II*** as a function of increasing shock obliquity (shock obliquity increasing from left to right).

Incipient regions of strain localization as shown in figure 9 for specimen ***II*** indicate large areas of damage-affected material. Using the kernel-average misorientation (KAM map), one can identify multiple "seeds" for such localization. Due to their proximity, these seeds begin to interact with each other creating large deformation-affected zones offering multiple void nucleation sites. Such highly disturbed regions, with intragranular orientation gradients of up to 45°, lead to multiple voids nucleating and growing simultaneously.

The influence of shock obliquity on shock hardening in specimen ***II*** was probed by measuring the diamond-pyramid hardness of the Ta sample 1mm below the loading surface as a function of run distance along the sample length. In figure 10 the hardness is seen to increase as a function of run distance(shock wave obliquity). Increasing hardness as a function of run distance subjected to sweeping-detonation-wave loading is thought to reflect a higher dislocation density consistent with increasing shear stresses with obliquity. Increasing shear stresses as a function of obliquity while the "hydrostatic pressure" portion of the imposed stress tensor decreases is the same trend as previously shown in Ta twinning studies of sweeping-wave loading and supported by modeling[11].

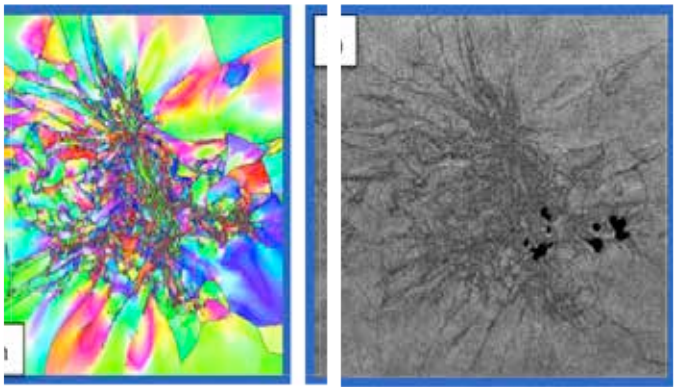

Fig. 7. Incipient damage région in spécimen II showing damaged région in a) crystal orientation and b) SEM detector signal maps. The orientation triangle is the same as in Fig. 5.

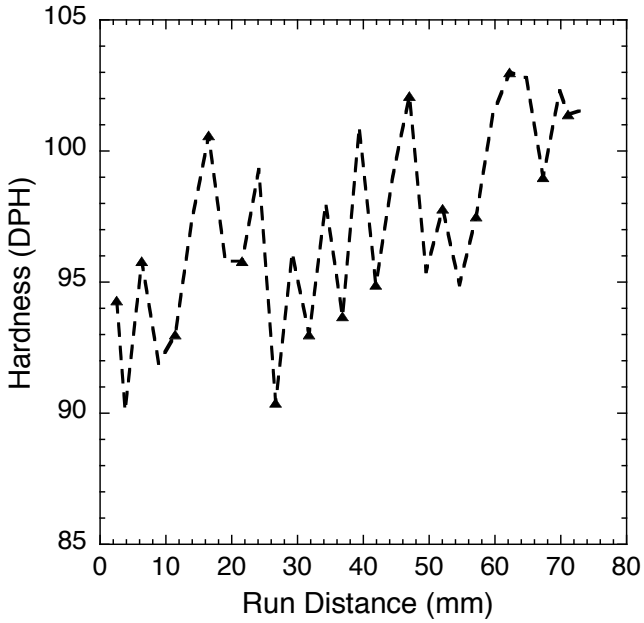

Fig. 8. Hardness measurements of specimen ***II*** as a function of detonation run distance along the sample reflecting the effect of shock obliquity on shock hardening.

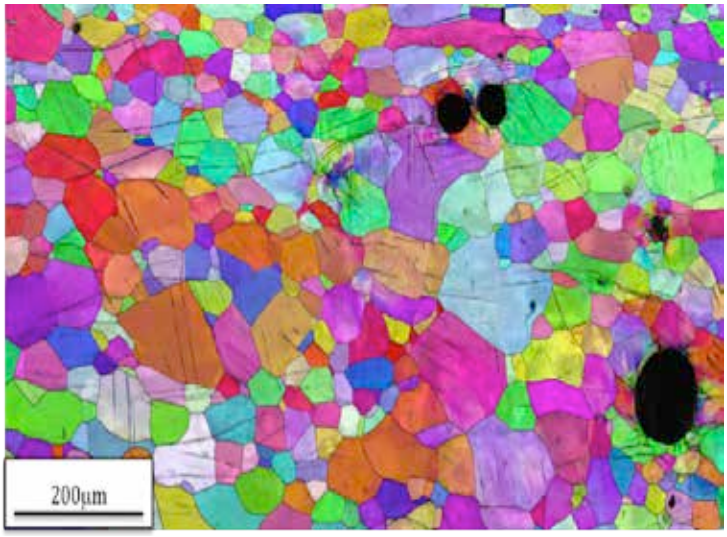

Fig. 9. Incipient damage in specimen ***III*** showing damage evolution below the main spall scab opening. The orientation triangle is the same as given in Fig. 5.

Removing the interlayer of foam in specimen ***III*** was seen to result in a single opened scab layer as well as a gradient of additional voids, void coalescence, shear localization, and cracking damage as a function of position from initiation of the sweeping wave. Figure 9 reveals a high density of fine deformation twins. Also observed, but not shown here, were large misorientations present below the opened scab fracture region after the sweeping wave was well established; i.e., approximately 2/3 down the length of the sample. The high volume fraction of grains in which twins were activated is similar to previous observations of the influence of shock obliquity on the imposed local shear stresses in the Ta as previously documented[11].

3.1b Post-Mortem Metallurgical Analysis – Curved-Plate Geometry

The damage evolution in energetic-driven oblique shock loading of the curved-plate Ta geometry was seen to vary as a function of obliquity and exhibit significant differences from the flat-plate incipient spall damaged specimen I, driven with the identical amount of HE, as seen in Figure 10. The curved Ta sample displays incipient void formation, a higher fraction (wider zone) of the sample area showing extensive void coalescence, and crack linkages as detailed in Figures 11 and 12 for the three areas delineated in Figure 10. The extent of evolved damage is seen to be both broader in width of the total sample thickness and more extensive than that observed for the flat-plate geometry sweeping wave, specimen *I*, for the equivalent amount of HE. This increased extent of overall damage displayed in the curved Ta sample compared to the flat-plate specimen is consistent with the rising level of shear with increasing obliquity, as discussed for the flat-plate, but suggests that the curved geometry, adding a convergent component to the sweeping wave, is also crucial to understanding the damage evolution. Clearly the increased damage evolved is on the one hand fully consistent with the increased shear imposed by the obliquity of the sweeping wave, but simultaneously inconsistent with the lack of increased deformation twin activation in the curved plate geometry as previously documented in the flat-plate. These two observations suggest a complex coupling and importance to both the obliquity and sample geometry when trying to understand the evolved damage evolution. Modeling of the curved plate-geometry spall experiment is in progress. This modeling will probe if accounting for the full stress tensor for the sweeping wave, in addition to the sample geometry, will yield insights into the observed increased damage evolution in the curved spall geometry. In addition, quantification of the hardness as a function of obliquity in the curved-plate geometry will be assessed.

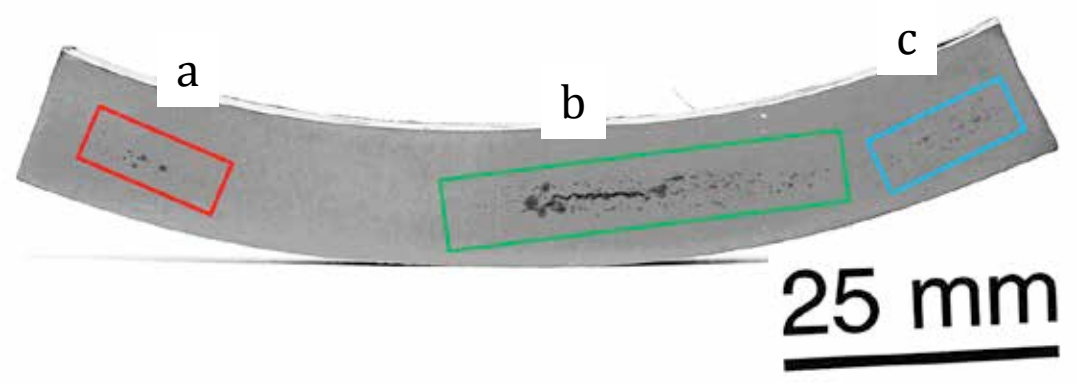

Figure 10. Macroscopic cross-sectional view of the curved sweeping detonation-wave sample using 8mm of Detasheet with a 6.35-mm foam interlayer revealing extensive evolved damage that increases with shock obliquity. The direction of the sweeping wave is from left to right in the sample, with the explosive applied on the bottom surface (converging geometry).

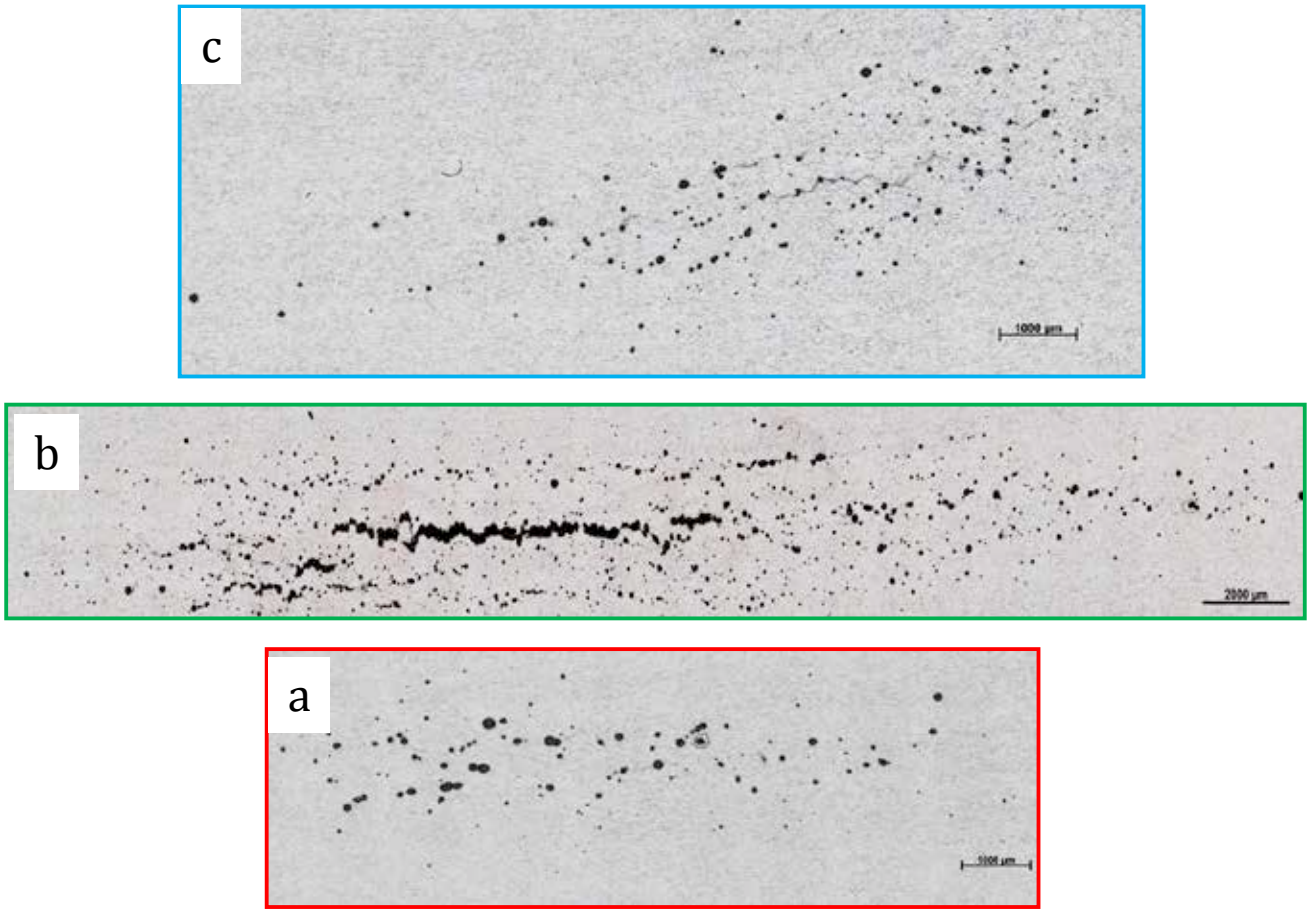

Figure 11. Higher magnification of the cross-sectional areas labeled in Figure 10.

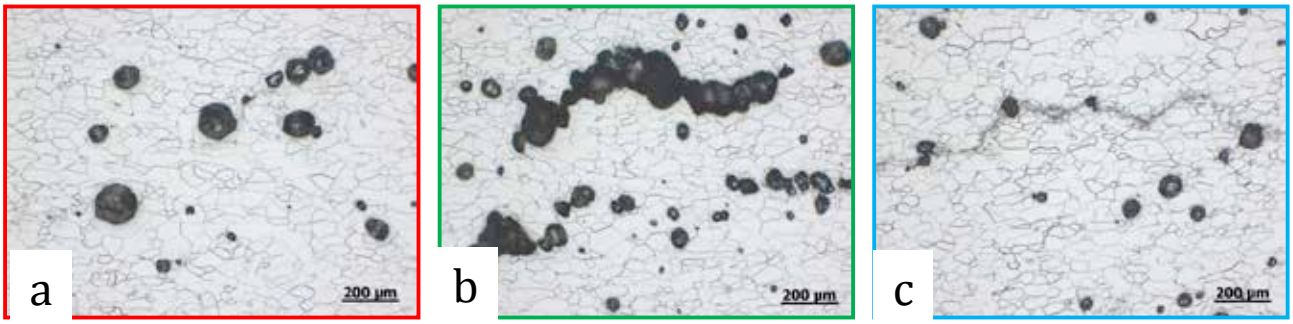

Figure 12. Higher magnification etched optical micrographs of the details of the damage evolution for cross-sectional areas labeled in Figure 10.

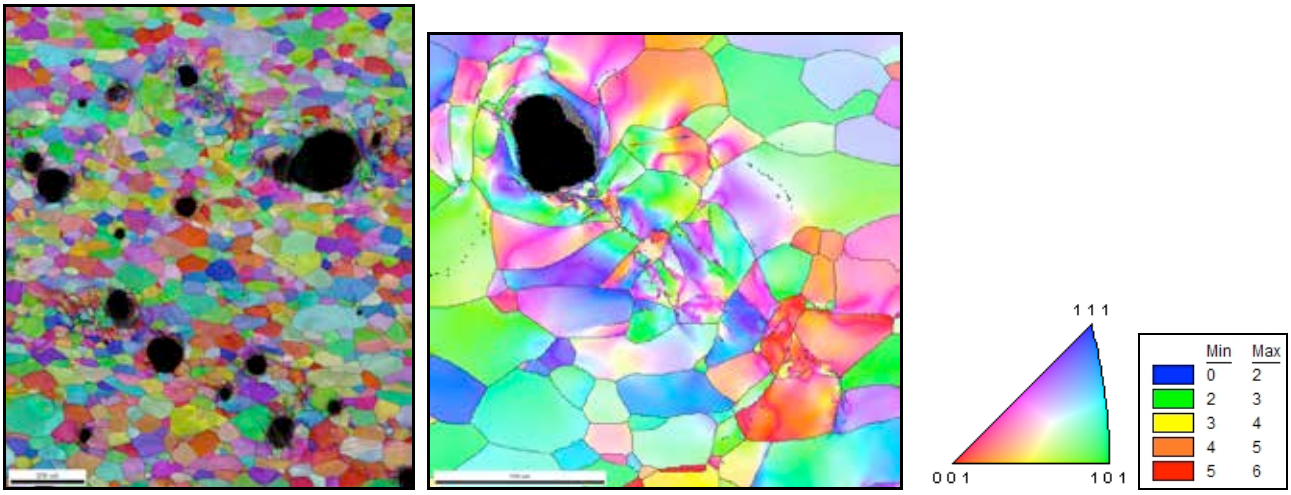

Figure 13. EBSD micrographs showing localized deformation linking separate voids with minimal coalescence from region "a" from the cross-sectional areas labeled in Figure 10.

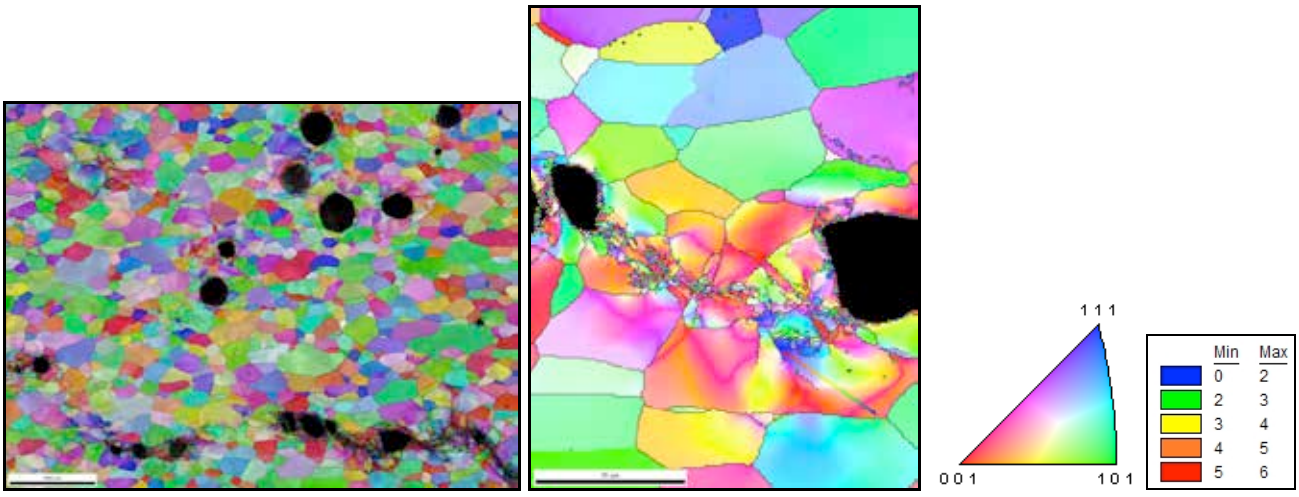

Figure 14. EBSD micrographs showing localized deformation linking separate voids with minimal coalescence from region "b" from the cross-sectional areas labeled in Figure 10.

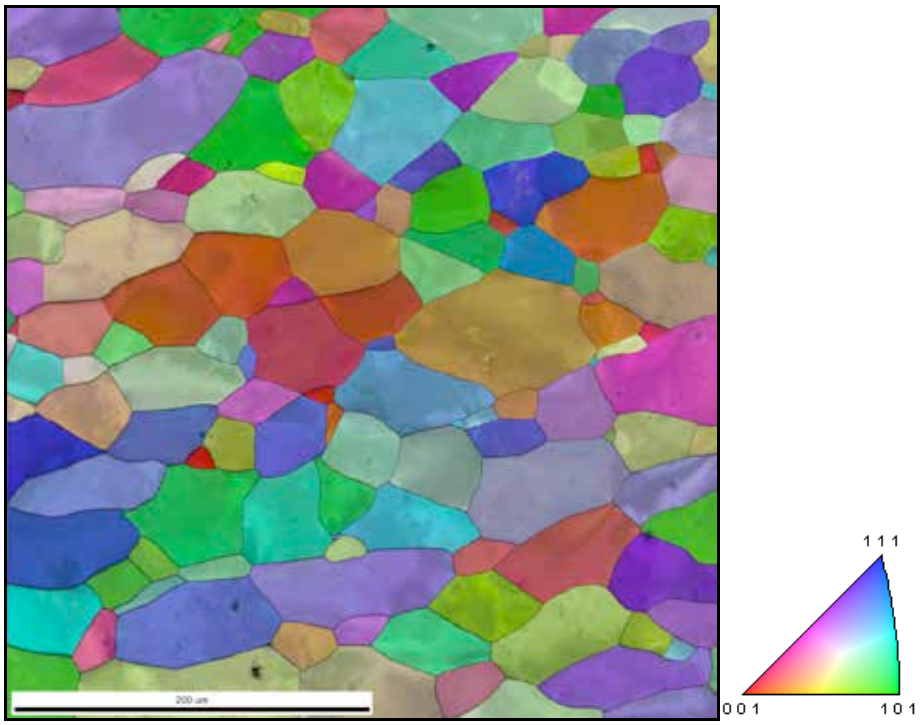

Figure 15. EBSD micrograph showing lack of deformation twinning in contrast to the extensive twinning displayed in the sweeping-wave flat-plate sample.

3.2a Velocimetry – Flat-Plate

The PDV data for the three Ta sweeping-detonation-wave spallation experiments is presented in figure 16. The wave profiles for the three experiments are seen to vary as a function of the foam thickness for a fixed 8mm of Detasheet of explosive. The effect of the removal of the foam in specimen ***III*** compared to specimens ***I*** and ***II*** is evident in the increase of the jump-off velocity. As a result, the velocity achieved by each plate should be nominally the same because the foam thickness variation is small. The in-contact experiment, specimen ***III***, shows a much higher "ultimate" velocity. This is because the plate spalled in this experiment. It should be noted that the velocity of the Hugoniot Elastic Limit(HEL) did not vary appreciably between the three experiments, but the character of the pull back due to yielding appears to be different. Data on the induced transverse velocities developed in Specimen ***I*** experiment has been discussed previously[14]. Similar data exists for specimens ***II*** and ***III*** and is under analysis.

After the spall event, the velocimeter is measuring the velocity of the spall scab on the front surface rather than the entire sample. Conversely, in Specimens ***I*** and ***II*** the plate remained intact and the velocimeter measured the lower ultimate velocity. As a beginning to the analysis of the data, the compressive stress of the incident shock, the tensile stress (pressure) achieved in the first unloading pulse, the strain rate of the unloading pulse, and the thickness implied by the duration of the period of the first ring, may be extracted from one of the probes positioned normal to the original surface. The formulas used are:

$P = \rho_0 u_s u_p$ for the incident pressure,

$\sigma^* = \frac{1}{2}\rho_0 c_b \Delta u_{fs}$ for the spall strength,

$\dot{\varepsilon} = -\dot{u}_{fs}/(2c_b)$ for the strain rate just before spall occurs, and $h = \frac{\tau}{2}c_l$ for the implied thickness of the sample volume undergoing ringing. The Romanchenko correction[15] to the spall strength can be written as : $\Delta\sigma^* = \frac{h}{2}\left(\frac{dp}{dt}\right)\left(\frac{1}{c_b} - \frac{1}{c_l}\right)$ and the stress rate estimated from: $\frac{dp}{dt} = \rho_0 c_l \dot{\varepsilon}$; The equation of state used is $u_s = 3.402 + 1.22u_p$ with $u_p = u_{fs}/2$, $\rho_0 = 16.65 g/cm^3$, and $c_b = 3.498 mm/\mu s$. The results are presented in Table I.

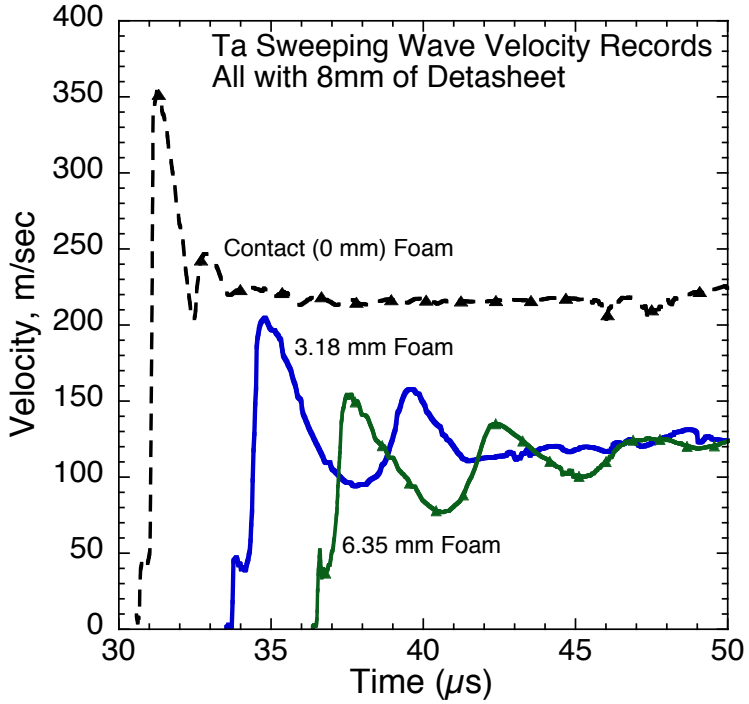

Figure 16. PDV wave profiles (particle velocity versus time plot) for the three sweeping-wave-spallation experiments.

Table I. Sweeping-Wave Spall Shot Data; (*Specimen III spalled ; the Romanchenko correction was only applied to this strength value)

Sample	Foam (mm)	Incident Shock, GPa	Tensile Spall Stress, GPa*	Strain Rate, s^{-1}	Ringing (mm)
I	6.35	4.5	2.6	$-4100$4100	9.6
II	3.18	6.0	3.8	$-161006$100	7.7
III	0	10.6	5.4	-124,000	2.5

Analysis of the recovered sample indicates that Specimen ***III*** drastically spalled, and the implied spall scab thickness of 2.5 mm is consistent with the post-shot observations. Analysis of the recovered sample in Specimen ***I*** showed very little microscopic damage and was nominally intact. The implied thickness of the material undergoing ringing is calculated to be 9.6 mm is just slightly less than the original sample thickness of 10.2 mm, and is also consistent with the post-shot and metallographic observations. Analysis of the recovered sample in Specimen ***II*** revealed some damage, but is also nominally intact. However, the implied thickness of the material undergoing ringing is calculated to be 7.7 mm, which is significantly less than the original sample thickness. The first period of the ringing of the velocity in Specimen ***II*** appears to have been interrupted early, and this interruption is responsible for the calculated intermediate thickness value. This disruption occurs before edge rarefactions should arrive, and is therefore likely associated with waves originating from damaged regions within the material, possibly from locations offset from the probe location. This analysis is consistent with the optical metallographic observation of a partially-formed spall plane and void coalescence in specimen ***II***.

Finally, the experiment that showed pronounced spall, specimen ***III***, developed a tensile stress (spall strength of ~5.4 GPa for a 10.6 GPa applied peak shock stress) below that quantified in previous studies of spallation in tantalum at equivalent peak shock stresses [16 , 17 , 18, 19 , 20]. Previous 1D loading experiments have documented spall strengths of 5.2 GPa for a 6 GPa shock amplitude, a 7.3 GPa spall strength for a peak shock stress of 9.5 GPa[19, 20], a spall strength of 6.2 GPa after shock compression to 19 GPa[21], and a spall strength of 8.1 GPa Under quasi-isentropic loading to 60 GPa [18]. The lower apparent spall strength observed during sweeping-wave loading is postulated to reflect a change in the damage evolution in Ta from essentially pure void nucleation and growth to a higher contribution of shear-damage processes consistent with the increased imposed shear stresses commensurate with the increased shear stresses, shock hardening, and increased twin formation propensity as a function of shock obliquity[11]. A higher propensity for twin formation with increasing obliquity coupled with the previous correlation of twins with void nucleation, may provide a plausible mechanism towards lowering spall strength for a sweeping wave compared to supported shock loading. Further study is required to quantitatively identify the physical processes responsible for this decrease in spall strength.

3.2b Velocimetry – Curved Plate Geometry

Figures 17 and 18 present the orthogonal (probes 1-6) and probes (7-12) angled 45 degrees to the curved spall specimen.

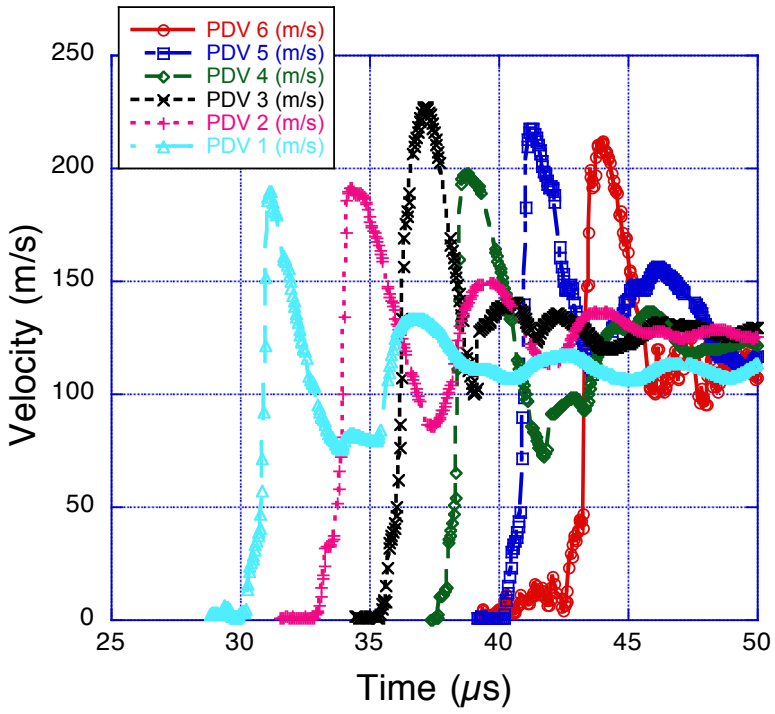

Figure 17. PDV wave profiles history (particle velocity versus time plot) for probes 1-6 (probes orthogonal to spot on curved surface) for the curved Ta plate spall experiment.

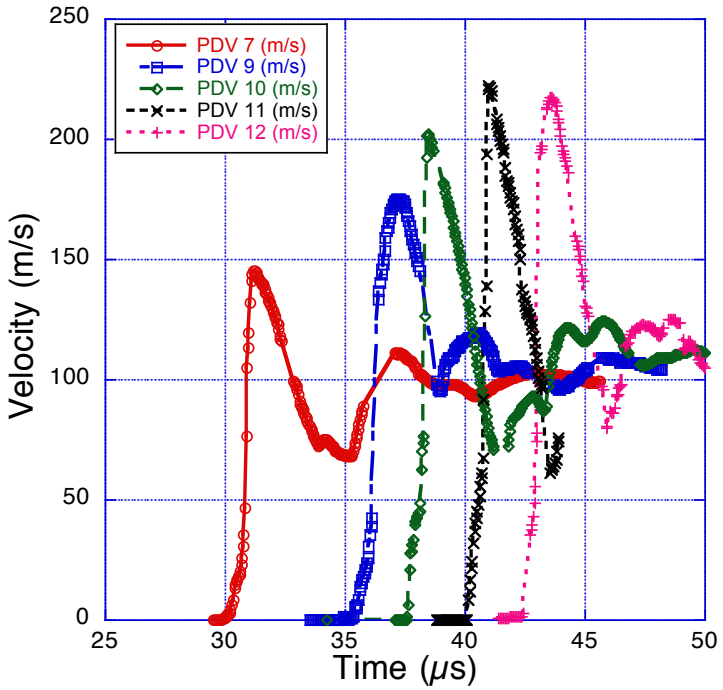

Figure 18. PDV wave profiles history (particle velocity versus time plot) for probes 7-12 (probes nominally at 45 degrees to spot on curved surface to register shear displacement) for the curved Ta plate spall experiment. (note – no data for probe 8 was obtained)

The extraction of the velocity-time curves, Figures 17 and 18, then provide the necessary input to estimate the particle velocity of the incident oblique shock. The analysis begins with finding the angle of the total velocity vector, as shown in Fig. 19, where the angle between the probes, ϕ, is known and one probe is aligned with the surface normal.

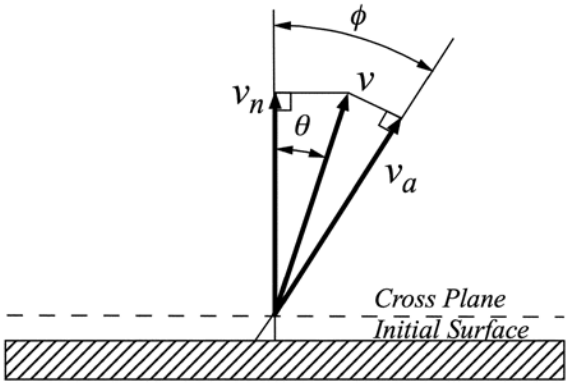

Figure 19 : Angled and normal PDV probe configuration.

$$v_n = v\cos\theta$$
$$v_a = v\cos(\phi - \theta)$$
$$\frac{v_a}{v_n} = \frac{\cos(\phi - \theta)}{\cos\theta} = \cos\phi + \sin\phi\tan\theta$$
$$\tan\theta = \frac{{}^{v_a}/_{v_n} - \cos\phi}{\sin\phi}$$

Consider a mass element on (very near to) the free surface with some initial velocity, presumed to be the particle velocity imparted by the shock, which is once again accelerated by the rarefaction reflected from the free surface. The rarefaction applies an impulse that alters both the magnitude and direction of the velocity of the mass element. Because the surface of the metal is flat, it is expected that the velocity change normal to the surface due to the impulse from the rarefaction will be approximately equal to the particle velocity behind the shock. Thus, we have :

$$u_{fs} = u_p + \overline{\Delta u} \qquad \text{(A1)}$$

and the component normal to the surface is :

$$u_{fs}\cos\theta = u_p\cos\alpha + u_p \qquad \text{(A2)}$$

where we have assumed $\Delta u_n = u_p$ (see the lower portion of Fig. 20). The angle of the free surface velocity vector, θ, is known from measurement relative to the free surface normal and the angle of interaction, α, is the angle between the tangent to the shock front and the tangent of the free surface. The equation for the normal component is immediately solved to give the desired formula :

$$\frac{u_{fs}}{u_p} = \frac{1 + \cos\alpha}{\cos\theta} \qquad \text{(A)}$$

Equation A is seen to interpolate the expected limits. When the shock wave interacts with the free surface at $\alpha = 0$, since θ 0, we get the Walsh "mirror" approximation, $u_{fs} = 2u_p$. When $\alpha = \pi/2$ we have u_{fs} $u_p/\cos\theta \approx \sqrt{2}u_p$ since $\theta \approx \pi/4$. The sweeping wave limit expresses the rule of thumb that sweeping shock waves accelerate metal as if the pressure were less than the actual pressure.

Equation A is approximate (e. g. material strength was neglected). In the experiment reported in this work, the crossed PDV probes are analyzed to obtain u_{fs} and θ. To estimate α, we may introduce the steady sweeping wave configuration, Fig. 20, along with the shock Hugoniot.

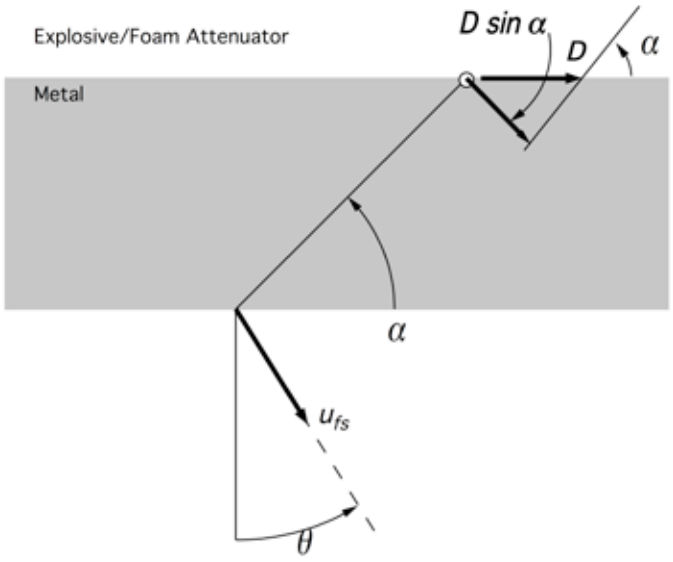

Figure 20: Schematic of analysis geometry for PDV data analysis

Summary:

Det. Velocity of detasheet

$D = 7.1$

Hugoniot of the metal (Ta $c_0 = 3.43, s = 1.19$)

$u_s = c_0 + s u_p$

Steady (quasi) wave approximation

$u_s = D \sin\alpha$

$D \sin\alpha = c_0 + s u_p$

$$u_p = \frac{D \sin\alpha - c_0}{s}$$

Free surface reflection

$$\frac{u_p}{u_{fs}} = \frac{\cos\theta}{1+\cos\alpha}$$

Combining

$$\frac{D \sin\alpha - c_0}{s} = \frac{u_{fs}\cos\theta}{1+\cos\alpha}$$

$$\left(\sin\alpha - \frac{c_0}{D}\right)(1+\cos\alpha) = \frac{s u_{fs}\cos\theta}{D}$$

which determines α in terms of the PDV-measured u_{fs}, θ, and the properties of the metal and explosive.

Table II: Curved sweeping wave experiment H4418.

Probe Pair	P-incident	Spall	Alpha
1 & 7	6.01	3.49	29.3
3 & 9	7.26	3.91	29.5
4&10	6.28	3.85	29.4
5& 11	7.08	4.94	29.3
6 & 12	6.74	3.35	29.5

α in degrees, P and σ_{spall} in GPa.

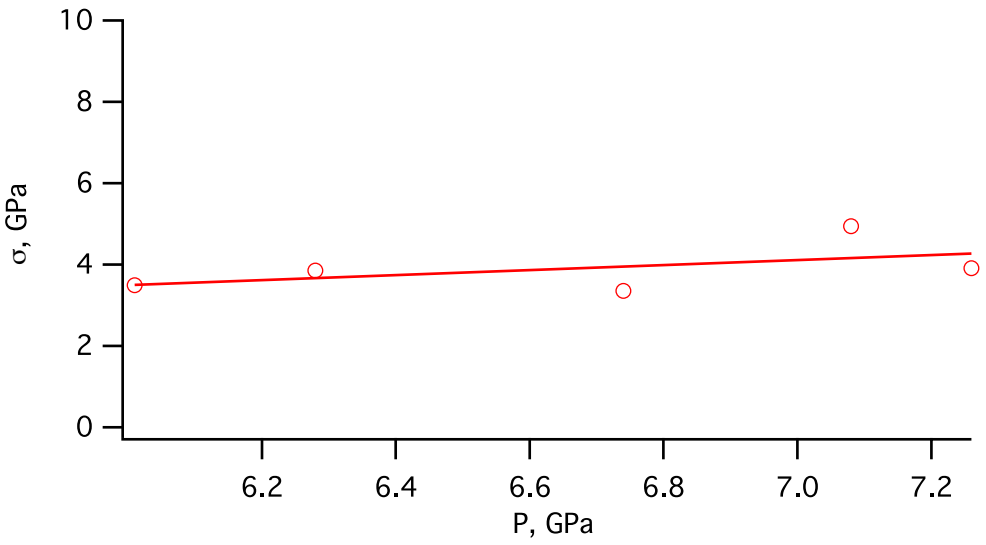

Figure 21: Spall strength versus Pressure for the Curved Plate Geometry

The spall stress seems to have a small variation with pressure, as presented in Figure 21, but the interaction angle does not vary with position. The pressure variation is thought to be due to variable foam thickness utilized between the datasheet and the Ta sample during assembly. From the perspective of the simple model, we have a steady wave process, and an average spall stress of 3.9 GPa, similar to the result for this foam thickness in the flat plate. The observed damage variation with run distance is presumed to be associated with the effect of shear caused by curvature or (total) turning angle in addition to the evolving obliquity with sweep run distance. Such an effect is not adequately captured by the simplified "first shock" theory presented here. The shear effect must be associated with the flow following the incident shocks.

On the other hand, if we use the angle θ as an indicator of the degree of shear, we see that with the exception of an outlier (which was near the edge of the sample), we have a general decrease in spall stress with increasing shear, as seen in Figure 22. This suggests a coupling of the increasing obliquity with the sweeping wave AND a contribution of the sample curvature. Continued analysis is in progress to more completely examine the details of this experiment and its correlation to the observed damage evolution. Incorporation of both the sample curvature and the sweeping wave into future modeling is planned.

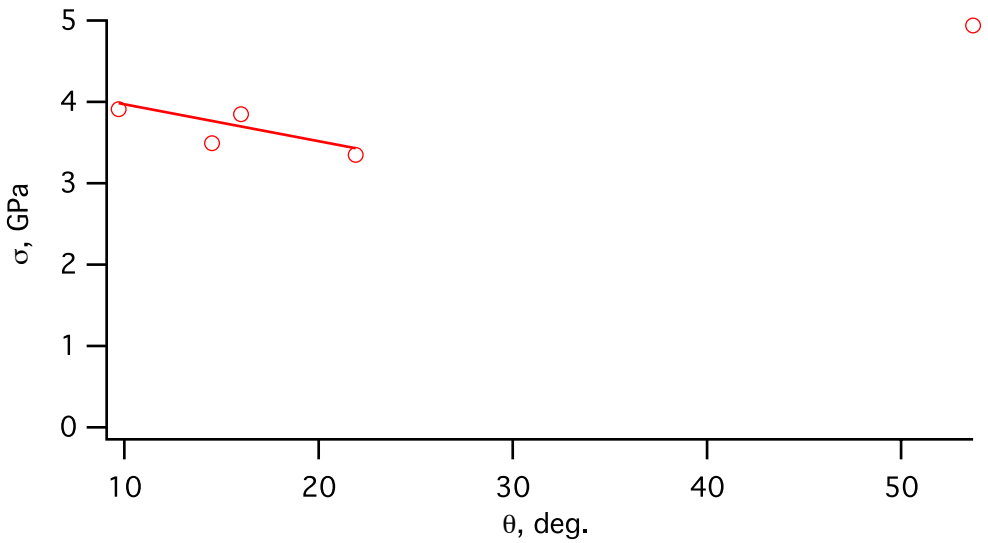

Figure 22: Spall strength versus θ for the Curved Plate Geometry

4 Summary

The spallation response of Ta is demonstrated to be critically dependent on the amplitude of the sweeping-shock-wave loading. Sweeping-wave loading is observed to: a) yield a lower spall strength than previously documented for 1-D supported-shock-wave loading with increasing obliquity in both the flat-plate and curved-plate geometries, b) exhibit increased shock hardening in the flat-plate as a function of increasing obliquity, and c) lead to increased incidence of deformation twin formation with shock obliquity in the flat-plate sweeping wave sample but NOT in the curved plate. Simplistic models of spallation, such as P_{min} based on 1-D square-top shock data lack the physics to capture the influence of kinetics on damage evolution such as that operative during sweeping detonation loading, let alone the coupling of a sweeping wave on a curved sample geometry. Quantification of the effects of shock

obliquity on defect generation and damage evolution in shock loaded materials is critical to the development of physically-based models of the shock response of condensed matter.

4 Future Work

Future efforts aimed at developing the basis for obtaining understanding of the effects of sweeping-wave shockwave loading on material behavior including when coupled with increasingly complex sample and/or component geometries includes:

a) complete detailed microstructural and PDV data analysis for the initial curved Ta sweeping wave assembly,

b) provide the data and specifics of the curved-plate Ta sweeping wave geometry to modelers to encourage and support computer simulations of this experiment in comparison and contrast with the flat-plate geometry to facilitate assessment of the accuracy of the physics in current codes,

c) conduct a similar curved-plate sweeping-wave experiment on Cu to compare with the flat-plate Cu sweeping-wave experimental data already completed;

d) compare and contrast the Cu cureved-sweeping-wave results with the current Ta data sets once completed; given that Cu exhibits enhanced shock hardening and Ta does not, the comparison will facilitate increased understanding of the combined synergies between material shockwave response, shockwave loading profile, and sample / component geometry.

Acknowledgements

Los Alamos National Laboratory is operated by Los Alamos National Security, LLC, for the National Nuclear Security Administration of the U.S. Department of Energy under contract DE-AC52-06NA25396. This work was partially sponsored by the Joint DoD/DOE Munitions Technology Development Program.

References

1. G. T. Gray III, N. K. Bourne, B. L. Henrie: J. Appl. Phys. **101,** 093507 (2007)
2. G. T. Gray III, L. M. Hull, J. R. Faulkner, M. E. Briggs, E. K. Cerreta, F. L. Addessio, N. K. Bourne, *Shock Compression of Condensed Matter-2009*(American Institute of Physics Press, 2009)
3. G. T. Gray III, V. Livescu, E. K. Cerreta: Matls. Sci. Forum **654-656,** 2297 (2010)
4. J. N. Johnson: J. Appl. Phys. **52,** 2812 (1981)
5. G. T. Gray III, N. K. Bourne, B. L. Henrie, J. C. F. Millett: J. Phys. IV France **110,** 773 (2003)
6. B. M. Butcher, L. M. Barker, D. E. Munson, C. D. Lundergan: AIAA Journal **2,** 977 (1964)
7. J. S. Rinehart: J. Appl. Phys. **23,** 1229 (1952)
8. L. V. Altshuler, S. A. Novikov, I. I. Divnov: Sov. Phys. Dokl. **11,** 79 (1966)
9. W. E. Drummond: J. Appl. Phys. **29,** 167 (1958)
10. V. A. Ogorodnikov, E. S. Tyunkin, A. A. Khokhlov, V. A. Grigorev, V. V. Mishukov: Strength Mater. **21,** 1207 (1989)

11. G. T. Gray III, V. Livescu, E. K. Cerreta, T. A. Mason, P. J. Maudlin, J. A. Bingert, *DYMAT 2009: 9th International Conference on the Mechanical and Physical Behaviour of Materials Under Dynamic Loading*(EDP Sciences, 2009)
12. B. L. Adams, S. I. Wright, K. Kunze: Metallurgical Transactions A **24A,** 819 (1993)
13. R. W. K. Honeycombe. *The Plastic Deformation of Metals*. Victoria, Australia: Edward Arnold Ltd., 1984
14. L. M. Hull, M. E. Briggs, J. R. Faulkner, *Shock Compression of Condensed Matter-2011*(in press., 2011)
15. V. I. Romanchenko, G. V. Stepanov: Strength Mater. **9,** 1110 (1977)
16. G. T. Gray III, In: *High Pressure Science and Technology 1993*, edited by Schmidt SC, Shaner JW, Samara GA, Ross M, American Institute of Physics, New York(1994), p.1103.
17. J. N. Johnson, R. S. Hixson, D. L. Tonks, A. K. Zurek, In: *Shock Compression of Condensed Matter 1995*, edited by Schmidt SC, Tao WC, American Institute of Physics, Woodbury, New York(1996), p.523.
18. L. C. Chhabildas, J. R. Asay, In: *Shock-Wave and High-Strain-Rate Phenomena in Materials*, edited by Meyers MA, Murr LE, Staudhammer KP, Marcel-Dekker, New York(1992), p.947.
19. G. T. Gray III, A. D. Rollett, In: *High Strain Rate Behavior of Refractory Metals and Alloys*, edited by Asfahani R, Chen E, Crowson A, The Minerals, Metals and Materials Society, Warrendale, Pennsylvania(1992), p.303.
20. A. K. Zurek, W. R. Thissell, J. N. Johnson, D. L. Tonks, R. Hixson: J. Mater. Process. Technol. **60,** 261 (1996)
21. L. C. Chhabildas, L. M. Barker, J. R. Asay, T. G. Trucano, In: *Shock Compression of Condensed Matter - 1989*, edited by Schmidt SC, Johnson JN, Davidson LW, Elsevier, Amsterdam(1990), p.429.